AIAA Aviation
22-26 June 2015, Dallas, TX
22nd AIAA Computational Fluid Dynamics Conference

Development of Generalized Summation-by-Parts Operators for the Second Derivative With a Variable Coefficient

David C. Del Rey Fernández* and David W. Zingg†
University of Toronto, Toronto, Ontario, M3H 5T6, Canada

The generalized summation-by-parts (GSBP) framework enables the derivation of novel and potentially efficient provably stable high-order finite-difference operators, applicable on general nodal distributions. This paper explores the application of GSBP operators to the solution of partial differential equations with first- and second-derivative terms. Here, we investigate compatible and order-matched GSBP operators for the approximation of the second derivative with a variable coefficient. These operators are one order more accurate than the application of the first-derivative operator twice and more dissipative of under-resolved modes. Several example operators are described in detail. To characterize the various operators, the steady linear convection-diffusion equation with a variable coefficient is solved.

I. Introduction

In this paper, we develop the generalized summation-by-parts (GSBP) method for the solution of partial differential equations (PDEs) that contain first-, second-, and mixed-derivative terms. The GSBP framework for the first derivative was developed by Del Rey Fernández et al.,[1] extended to temporal terms by Boom and Zingg,[2,3] and to approximations of the second derivative with a variable coefficient by Del Rey Fernández and Zingg.[4] The GSBP framework is based on extending the theory of the finite-difference summation-by-parts (SBP) operators of Kreiss and Scherer,[5] and Strand,[6] which we denote *classical* SBP operators, to a broader class of operators with one or more of the following characteristics: i) a non-repeating interior point operator, ii) a non-uniform nodal distribution, and iii) the exclusion of one or both boundary nodes. Boundary conditions and inter-element coupling can be weakly enforced using simultaneous approximation terms (SATs).[7–14] The SBP-SAT approach leads to consistent, conservative, and provably stable discretizations of PDEs; the generalized framework extends these properties to a wide range of operators.

One of the main difficulties in the development of high-order methods is the construction of numerical boundary operators that lead to stable methods. The SBP-SAT approach alleviates this difficulty by providing a tractable means of developing high-order methods that are provably time stable. For a certain class of PDEs, it is possible to use the energy method to determine the conditions under which the PDE and a set of initial and boundary conditions lead to a stable problem and, if a unique solution exists, a well-posed problem.[15–17] In the SBP-SAT approach, boundary and initial conditions are modelled after the continuous boundary and initial conditions that lead to a stable problem. Then, in a one-to-one fashion to the continuous analysis, the discrete-energy method is applied to determine the conditions under which the numerical boundary and initial conditions lead to stability. These same ideas can then be applied to inter-block coupling SATs. The key that allows this one-to-one relationship is that SBP operators mimic the integration-by-parts property of the continuous PDE. Another benefit of the SBP-SAT approach is that the requirement for grid continuity between elements or blocks is at most $\mathcal{C}^0$. This is advantageous as it significantly reduces the difficulty in constructing a mesh around complex geometries. The GSBP framework extends the SBP-SAT approach for classical SBP operators to a larger family of operators, which is beneficial

*Ph.D. candidate, Institute for Aerospace Studies, 4925 Dufferin St., and AIAA Student Member (dcdelrey@oddjob.utias.utoronto.ca)
†Professor and Director, J. Armand Bombardier Foundation Chair in Aerospace Flight, Institute for Aerospace Studies, 4925 Dufferin St., and AIAA Member Grade.

for two principal reasons. First, GSBP operators exist that potentially lead to more efficient discretizations compared to classical SBP operators.[4,18] Second, GSBP element-type operators exist that, for a given order of accuracy, require fewer nodes than classical SBP operators. This can be advantageous in tessellating regions with significant geometric variation. For such regions, it is preferable to use a large number of small elements with modest numbers of nodes. In this way, when applying the operators in curvilinear co-ordinates, the metric Jacobians have a smaller probability of causing numerical issues.

The focus of this paper is on diagonal-norm GSBP approximations to the second derivative that are more accurate than the application of the first-derivative operator twice. The GSBP first-derivative operator has the form $\mathsf{D}_1 = \mathsf{H}^{-1}\mathsf{Q}$, where the symmetric positive definite matrix H is known as the norm matrix and can be either diagonal or dense. However, we do not discuss dense-norm operators since it is unclear how to construct second-derivative operators using dense-norm operators that lead to stable discretizations without an ad hoc procedure; for example, see Mattsson and Almquist.[19] GSBP operators that are one order more accurate than the application of the first-derivative operator twice, denoted order-matched, and compatible with GSBP operators approximating mixed-derivative terms—meaning that they lead to stable discretizations when such terms are present—have been developed by Del Rey Fernández and Zingg.[4] Here, we have two objectives. First, we provide a brief overview of GSBP operators as well as a detailed account of how to implement such operators. Second, we showcase the efficiency gains that can be obtained by using GSBP operators.

This paper is organized as follows: Section II introduces the notation used in this paper. We then explain the two classes of GSBP operators considered in this paper in Section III. A brief review of GSBP operators for the first and second derivatives is given in Section IV. In Section V, we show how to discretize the linear convection-diffusion equation with a variable coefficient using GSBP operators and SATs for the imposition of boundary conditions. A summary of the GSBP operators considered in this paper is given in Section VI. Various GSBP operators are characterized by solving the linear convection-diffusion equation in Section VII. Finally, conclusions are drawn in Section VIII.

II. Notation

Vectors are denoted with small bold letters, for example, $\mathbf{x} = [x_1, \ldots, x_n]^{\mathrm{T}}$, while matrices are presented using capital letters with sans-serif font, for example, M. Capital letters with script type are used to denote continuous functions on a specified domain $x \in [x_{\mathrm{L}}, x_{\mathrm{R}}]$. As an example, $\mathcal{U}(x) \in C^{\infty}[x_{\mathrm{L}}, x_{\mathrm{R}}]$ denotes an infinitely differentiable function on the domain $x \in [x_{\mathrm{L}}, x_{\mathrm{R}}]$. Lower case bold font is used to denote the restriction of such functions onto a grid; for example, the restriction of $\mathcal{U}$ onto the grid $\mathbf{x}$ is given by

$$\mathbf{u} = [\mathcal{U}(x_1), \ldots, \mathcal{U}(x_n)]^{\mathrm{T}}. \tag{1}$$

Vectors with a subscript h, for example, $\mathbf{u}_h \in \mathbb{R}^{n\times 1}$, represent the solution to the discrete or semi-discrete problem.

The restriction of monomials onto a set of nodes is used throughout this paper and is represented by $\mathbf{x}^k = \left[x_1^k, \ldots, x_n^k\right]^{\mathrm{T}}$, with the convention that $\mathbf{x}^k = 0$ if $k < 0$. A subscript is used to denote which derivative is being approximated. For example, D_1 denotes an SBP approximation to the first derivative. The second derivative can be approximated by applying an SBP operator approximating the first derivative twice or by constructing SBP operators that have preferential properties. For this latter type, it is necessary to differentiate between approximations of the constant-coefficient derivative and the variable-coefficient derivative. We use D_2 to denote an SBP approximation to the constant-coefficient second derivative, while $\mathsf{D}_2(\mathsf{B})$ represents the approximation to the second derivative with variable coefficients $\mathcal{B}$, where $\mathsf{B} = \mathrm{diag}[\mathcal{B}(x_1), \ldots, \mathcal{B}(x_n)]$ and $\mathcal{B}$ is the variable coefficient. We discuss the degree of SBP operators, that is, the degree of monomial for which they are exact, as well as the order of the operators. The approximation of the derivative has a leading truncation error term for each node, proportional to some power of h. The order of the operator is taken as the smallest exponent of h in these truncation errors. The relation between the order and degree of an operator approximating the m^{th} derivative is

$$\text{order} = \text{degree} - m + 1. \tag{2}$$

III. Element-type operators vs. operators with a repeating interior point operator

In this paper, we consider two classes of GSBP operators, element-type operators and operators with a repeating interior point operator. Element-type operators exist on nodal distributions of fixed size, and the domain is discretized by dividing the domain into a number of elements. Then, mesh refinement is carried out using the *element approach* whereby each element is subdivided. For example, consider the following four-node element-type GSBP operator for the second derivative on $x \in [x_{\mathrm{L}}, x_{\mathrm{R}}]$, constructed by applying the first-derivative operator twice:

$$\mathsf{D}_2 = \tfrac{4}{(x_{\mathrm{R}}-x_{\mathrm{L}})^2} \begin{bmatrix} 5 & -\frac{5}{4}-\frac{15\sqrt{5}}{4} & -\frac{5}{4}+\frac{15\sqrt{5}}{4} & -\frac{5}{2} \\ \frac{3}{4}\sqrt{5}+\frac{5}{4} & -5 & \frac{5}{2} & \frac{5}{4}-\frac{3}{4}\sqrt{5} \\ \frac{5}{4}-\frac{3}{4}\sqrt{5} & \frac{5}{2} & -5 & \frac{3}{4}\sqrt{5}+\frac{5}{4} \\ -\frac{5}{2} & -\frac{5}{4}+\frac{15\sqrt{5}}{4} & -\frac{5}{4}-\frac{15\sqrt{5}}{4} & 5 \end{bmatrix}. \tag{3}$$

This operator is of order two and approximates the second derivative on the Legendre-Gauss-Lobatto nodes, which after transformation from the canonical domain $\tilde{x} \in [-1, 1]$ to $x \in [x_{\mathrm{L}}, x_{\mathrm{R}}]$, are given by

$$\mathbf{x} = \frac{x_{\mathrm{R}} - x_{\mathrm{L}}}{2} \begin{bmatrix} -1 & -\frac{1}{5}\sqrt{5} & \frac{1}{5}\sqrt{5} & 1 \end{bmatrix}^{\mathrm{T}} + \frac{x_{\mathrm{R}} + x_{\mathrm{L}}}{2}. \tag{4}$$

On a mesh with m equally sized elements on the domain $x \in [x_{\mathrm{L}}, x_{\mathrm{R}}]$, the operator becomes:

$$\frac{4\,m^2}{(x_{\mathrm{R}} - x_{\mathrm{L}})^2} \begin{bmatrix} \mathsf{D}_2 & & \\ & \ddots & \\ & & \mathsf{D}_2 \end{bmatrix}. \tag{5}$$

To understand an operator with a repeating interior point operator, consider the following SBP operator applied on a nodal distribution with n equally-spaced nodes:

$$\mathsf{D}_2 = \frac{(n-1)^2}{(x_{\mathrm{R}} - x_{\mathrm{L}})^2} \begin{bmatrix} d_{11} & d_{12} & d_{13} & d_{14} & & & & & & \\ d_{21} & d_{22} & d_{23} & d_{24} & & & & & & \\ d_{31} & d_{32} & d_{33} & d_{34} & d_{35} & & & & & \\ d_{41} & d_{42} & d_{43} & d_{44} & d_{45} & d_{46} & & & & \\ & & -\frac{1}{12} & \frac{4}{3} & -\frac{4}{2} & \frac{4}{3} & -\frac{1}{12} & & & \\ & & & \ddots & \ddots & \ddots & \ddots & \ddots & & \\ & & & & -\frac{1}{12} & \frac{4}{3} & -\frac{4}{2} & \frac{4}{3} & -\frac{1}{12} & \\ & & & & & d_{46} & d_{45} & d_{43} & d_{42} & d_{41} \\ & & & & & d_{35} & d_{34} & d_{32} & d_{32} & d_{31} \\ & & & & & & d_{24} & d_{23} & d_{22} & d_{21} \\ & & & & & & d_{14} & d_{13} & d_{12} & d_{11} \end{bmatrix}. \tag{6}$$

The repeating interior point operator is $\frac{(n-1)^2}{(x_{\mathrm{R}}-x_{\mathrm{L}})^2} \begin{bmatrix} -\frac{1}{12} & \frac{4}{3} & -\frac{4}{2} & \frac{4}{3} & -\frac{1}{12} \end{bmatrix}$ and is a fourth-order approximation to the second derivative. There are boundary point operators at the first and last four nodes which have coefficients d_{ij}. With such an operator, mesh refinement is accomplished using the *traditional finite-difference approach* where the number of nodes at which the interior point operator is applied is increased. Note that one can also fix the size of such an operator and apply it using the element approach. We use element through this paper and only use block when the difference is important.

IV. Generalized summation-by-parts operators for the first and second derivatives

For the first derivative, a GSBP operator is defined as

Definition 1 Generalized summation-by-parts operator: *A matrix operator* $\mathsf{D}_1 \in \mathbb{R}^{n\times n}$ *of order* p *is an approximation to the first derivative, on the nodal distribution* $\mathbf{x}$ *that need neither be uniform nor include nodes on the boundaries and may have nodes that lay outside of the domain of the element* $x \in [x_\mathrm{L}, x_\mathrm{R}]$*, with the SBP property if it satisfies the equations*

$$\mathsf{D}_1 \mathbf{x}^j = j\mathbf{x}^{j-1},\ j \in [0, p], \tag{7}$$

and is of the form

$$\mathsf{D}_1 = \mathsf{H}^{-1}\mathsf{Q}, \tag{8}$$

where H*, which is referred to as the norm matrix, is symmetric positive definite, and* $\mathsf{Q} + \mathsf{Q}^\mathrm{T} = \mathsf{E}$*, where* $\left(\mathbf{x}^i\right)^\mathrm{T} \mathsf{E}\mathbf{x}^j = x_\mathrm{R}^{i+j} - x_\mathrm{L}^{i+j}$*,* $i, j \in [0, r]$*,* $r \geq p$*.*

For later use, we note that $\mathsf{E} = \mathsf{E}_{x_\mathrm{R}} - \mathsf{E}_{x_\mathrm{L}}$, where

$$\begin{gathered} \mathsf{E}_{x_\mathrm{R}} = \mathbf{t}_{x_\mathrm{R}} \mathbf{t}_{x_\mathrm{R}}^\mathrm{T}, \qquad\qquad \mathsf{E}_{x_\mathrm{L}} = \mathbf{t}_{x_\mathrm{L}} \mathbf{t}_{x_\mathrm{L}}^\mathrm{T}, \\ \mathbf{t}_{x_\mathrm{R}} \mathbf{u} = \mathcal{U}(x_\mathrm{R}) + \mathcal{O}(h^{r+1}), \quad \mathbf{t}_{x_\mathrm{L}} \mathbf{u} = \mathcal{U}(x_\mathrm{L}) + \mathcal{O}(h^{r+1}). \end{gathered} \tag{9}$$

This is relevant if the nodal distribution does not include boundary nodes. If both boundary nodes are included, then $\mathsf{E} = \mathrm{diag}\,(-1, 0, \ldots, 0, 1)$.

For the second derivative, we can apply the first-derivative operator twice; this leads to discretizations that are provably stable using the energy method. However, for operators with a repeating interior point operator, this has the drawback that the interior point operator requires solution information from almost twice the number of nodes, as compared to the interior point operator of the first-derivative operator. Moreover, whether the first-derivative operator has a repeating interior point operator or is an element-type operator, the application of the first-derivative operator twice leads to an approximation of the second derivative that is one order less accurate than the first-derivative operator. Therefore, we search for GSBP operators that are one order more accurate than the application of the first-derivative operator twice. In addition, we only consider operators that are compatible with the first-derivative GSBP operator used to discretize the same spatial direction of mixed-derivative terms since such operators can be shown to lead to stable discretizations for PDEs that contain such terms.[12,20] The definition for the second-derivative GSBP operator we propose combines ideas from Refs. 11, 20, 12, and 21, and full details can be found in Del Rey Fernández and Zingg.[4]

Consider the following definition for a second-derivative GSBP operator:[4]

Definition 2 Compatible and order-matched second-derivative GSBP operator: *The matrix* $\mathsf{D}_2\,(\mathsf{B}) \in \mathbb{R}^{n\times n}$ *is a GSBP operator approximating the second derivative,* $\frac{\partial}{\partial x}\left(\mathcal{B}\frac{\partial \mathcal{U}}{\partial x}\right)$*, of order* p *that is compatible with the first-derivative GSBP operator* $\mathsf{D}_1 = \mathsf{H}^{-1}\mathsf{Q}$*, on a nodal distribution* $\mathbf{x}$*, if it satisfies the equations*

$$\mathsf{D}_2\left(diag\left(\mathbf{x}^k\right)\right)\mathbf{x}^s = s(k+s-1)\mathbf{x}^{k+s-2},\ k+s \leq p+1, \tag{10}$$

and is of the form

$$\mathsf{D}_2\,(\mathsf{B}) = \mathsf{H}^{-1}\left[-\mathsf{D}_1^\mathrm{T}\mathsf{H}\mathsf{B}\mathsf{D}_1 + \sum_{i=1}^{n} \mathsf{B}\,(i,i)\,\mathsf{R}_i + \mathsf{E}\mathsf{B}\tilde{\mathsf{D}}_1\right]. \tag{11}$$

The matrices R_i*,* B*, and* $\tilde{\mathsf{D}}_1$ *are* $\in \mathbb{R}^{n\times n}$*;* R_i *is symmetric negative semi-definite,*

$$\mathsf{B} = diag(\mathcal{B}(x_1), \ldots, \mathcal{B}(x_n)),$$

and $\tilde{\mathsf{D}}_1$ *is an approximation to the first derivative of order* $\geq p+1$*.*

For stability, the norms H of all operators in a given spatial direction must be the same. As a result, all first-derivative terms are typically approximated using the same GSBP operator.

The main difficulty in deriving compatible and order-matched GSBP operators is fulfilling the requirement that the R_i be symmetric negative semi-definite. Instead, we can leverage the compatible and order-matched GSBP operator for the constant-coefficient case, which is given as

$$\mathsf{D}_2 = \mathsf{H}^{-1}\left[-\mathsf{D}_1^\mathrm{T}\mathsf{H}\mathsf{D}_1 + \mathsf{R}_\mathrm{c} + \mathsf{E}\tilde{\mathsf{D}}_1\right] \tag{12}$$

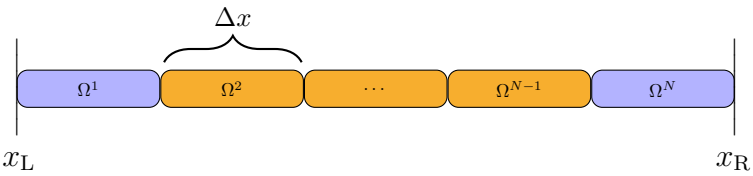

Figure 1: Tessellation of the domain Ω into N equally sized non-overlapping elements.

and construct the variable-coefficient operator as[4]

$$\mathsf{D}_2\left(\mathsf{B}\right) = \mathsf{H}^{-1}\left[-\mathsf{D}_1^{\mathrm{T}}\mathsf{H}\mathsf{B}\mathsf{D}_1 + \frac{\sum_{i=1}^{n}\mathsf{B}(i,i)}{n}\mathsf{R}_\mathrm{c} + \mathsf{E}\mathsf{B}\tilde{\mathsf{D}}_1\right]. \tag{13}$$

In this paper, we use form (13) to construct element-type GSBP operators for the second derivative. However, for practical implementation, it is more convenient to recast (13) or (11) in terms of the variable coefficient, which leads to

$$\mathsf{D}_2\left(\mathsf{B}\right) = \sum_{i=1}^{n}\mathsf{B}(i,i)\mathsf{M}_i. \tag{14}$$

This is the form that we use in presenting the operators as well as in the example in the next section.

V. Implementing the GSBP-SAT method

In this section, the mechanics of discretizing a steady PDE using the GSBP-SAT approach are exemplified by discretizing the linear convection-diffusion equation. We begin by discussing how to discretize the PDE, without reference to a particular set of GSBP operators. We then discuss SATs for GSBP operators that include boundary nodes and those that do not, using specific examples of such operators. Finally, we discuss the implementation of compatible and order-matched operators and an efficient means of implementing operators with a repeating interior point using the traditional finite-difference approach.

The continuous problem that we solve is given as

$$-a\frac{\partial \mathcal{U}}{\partial x} + \mu\frac{\partial}{\partial x}\left(\mathcal{B}\frac{\partial \mathcal{U}}{\partial x}\right) = 0, \quad x \in [x_\mathrm{L}, x_\mathrm{R}], \quad \mathcal{B} > 0, \text{ and, } a, \mu > 0. \tag{15}$$

The boundary conditions are given as

$$\alpha_{x_\mathrm{L}}\mathcal{U}_{x_\mathrm{L}} + \beta_{x_\mathrm{L}}\mathcal{B}_{x_\mathrm{L}}\left.\frac{\partial \mathcal{U}}{\partial x}\right|_{x_\mathrm{L}} = \mathcal{G}_{x_\mathrm{L}}, \ \alpha_{x_\mathrm{R}}\mathcal{U}_{x_\mathrm{R}} + \beta_{x_\mathrm{R}}\mathcal{B}_{x_\mathrm{R}}\left.\frac{\partial \mathcal{U}}{\partial x}\right|_{x_\mathrm{R}} = \mathcal{G}_{x_\mathrm{R}}, \tag{16}$$

where we use the notation $\mathcal{U}_{x_\mathrm{L}} = \mathcal{U}\left(x_\mathrm{L}\right)$, for example. For stability, the coefficients in (16) must satisfy the relations[22]

$$a + \frac{2\mu\alpha_{x_\mathrm{R}}}{\beta_{x_\mathrm{R}}} > 0, \quad a + \frac{2\mu\alpha_{x_\mathrm{L}}}{\beta_{x_\mathrm{L}}} < 0. \tag{17}$$

For operators with a repeating interior point operator, we can use the traditional finite-difference approach. In such a case, the discretization is given as

$$-a\mathsf{D}_1\mathbf{u}_h + \mu\mathsf{D}_2\left(\mathsf{B}\right)\mathbf{u}_h + \mathbf{SAT}_{x_\mathrm{L}} + \mathbf{SAT}_{x_\mathrm{R}} = 0. \tag{18}$$

The vectors $\mathbf{SAT}_{x_\mathrm{L}}$ and $\mathbf{SAT}_{x_\mathrm{R}}$ are the boundary SAT vectors. For the linear convection-diffusion equation they are given as

$$\begin{aligned}
\mathbf{SAT}_{x_\mathrm{L}} &= \sigma_{x_\mathrm{L}}\mathsf{H}^{-1}\mathsf{E}_{x_\mathrm{L}}\left(\alpha_{x_\mathrm{L}}\mathbf{u}_h + \beta_{x_\mathrm{L}}\mathsf{B}\tilde{\mathsf{D}}_1\mathbf{u}_h - g_{x_\mathrm{L}}\mathbf{1}\right) = \mathsf{SAT}_{x_\mathrm{L}}\mathbf{u}_h + g_{x_\mathrm{L}}\mathsf{SAT}_{\mathrm{BCL}}\mathbf{1}, \\
\mathbf{SAT}_{x_\mathrm{R}} &= \sigma_{x_\mathrm{R}}\mathsf{H}^{-1}\mathsf{E}_{x_\mathrm{R}}\left(\alpha_{x_\mathrm{R}}\mathbf{u}_h + \beta_{x_\mathrm{R}}\mathsf{B}\tilde{\mathsf{D}}_1\mathbf{u}_h - g_{x_\mathrm{R}}\mathbf{1}\right) = \mathsf{SAT}_{x_\mathrm{R}}\mathbf{u}_h + g_{x_\mathrm{R}}\mathsf{SAT}_{\mathrm{BCR}}\mathbf{1},
\end{aligned} \tag{19}$$

where $\mathsf{SAT}_{x_\mathrm{L}}$, $\mathsf{SAT}_{\mathrm{BCL}}$, $\mathsf{SAT}_{x_\mathrm{R}}$, and $\mathsf{SAT}_{\mathrm{BCR}}$, are $n \times n$ matrices. Furthermore, g_{x_R} and g_{x_L} are from the continuous boundary conditions, and $\mathbf{1}$ is a vector of ones. On close inspection of (19), we can see that the terms within the parentheses are modelled after the continuous boundary conditions. Rearranging (18), we obtain

$$\overbrace{\left[-a\mathsf{D}_1 + \mu\mathsf{D}_2\left(\mathsf{B}\right) + \mathsf{SAT}_{x_\mathrm{L}} + \mathsf{SAT}_{x_\mathrm{R}}\right]}^{\mathsf{A}} \mathbf{u}_h = \overbrace{-g_{x_\mathrm{L}}\mathsf{SAT}_{\mathrm{BCL}}\mathbf{1} - g_{x_\mathrm{R}}\mathsf{SAT}_{\mathrm{BCR}}\mathbf{1}}^{\mathbf{r}}. \tag{20}$$

The solution to (20) is given as

$$\mathbf{u}_h = \mathsf{A}^{-1}\mathbf{r}. \tag{21}$$

Alternatively, we divide the domain $\Omega = \{x | x \in [x_\mathrm{L}, x_\mathrm{R}]\}$ into N equally sized non-overlapping elements. Figure 1 displays this simple tessellation, where the partition is given as

$$\Omega^i = \left\{x | x \in \left[(i-1)\,\Delta x + x_\mathrm{L}, i\,\Delta x\right]\right\}, \quad i \in [1, N]$$

and $\Delta x = \frac{x_\mathrm{R} - x_\mathrm{L}}{N}$. The elements highlighted in blue, Ω^1 and Ω^N, are the elements where the numerical boundary operators must be applied. The remaining elements, highlighted in orange, require numerical interface procedures to couple the solution. If the nodal distribution within each element contains nodes at the element boundaries, then the global solution is multivalued at those nodes.

The discretization of (15) at the first element is given as

$$-a\mathsf{D}_1\mathbf{u}_h^1 + \mu\mathsf{D}_2(\mathsf{B}^1)\mathbf{u}_h^1 + \mathbf{SAT}_{x_\mathrm{L}} + \mathbf{SAT}_\mathrm{R}^1 = 0, \tag{22}$$

while for the last element, the discretization is given as

$$-a\mathsf{D}_1\mathbf{u}_h^N + \mu\mathsf{D}_2(\mathsf{B}^N)\mathbf{u}_h^N + \mathbf{SAT}_{x_\mathrm{R}} + \mathbf{SAT}_\mathrm{L}^N = 0. \tag{23}$$

The boundary SAT vectors are given by (19), where $\mathbf{u}_h$ and B are replace by $\mathbf{u}_h^1$ and B^1 for $\mathbf{SAT}_{x_\mathrm{L}}$ and $\mathbf{u}_h^N$ and B^N for $\mathbf{SAT}_{x_\mathrm{R}}$—we discuss the interface coupling SAT vectors, $\mathbf{SAT}_\mathrm{R}^1$ and $\mathbf{SAT}_\mathrm{L}^N$ below.

For the i^{th} element, $1 < i < N$, the discrete approximation to the PDE is given as

$$-a\mathsf{D}_1\mathbf{u}_h^i + \mathsf{D}_2\left(\mathsf{B}^i\right)\mathbf{u}_h^i + \mathbf{SAT}_\mathrm{L}^i + \mathbf{SAT}_\mathrm{R}^i = 0. \tag{24}$$

The SAT vectors couple the i^{th} element to the $(i-1)^{\text{th}}$ and $(i+1)^{\text{th}}$ elements and can generically be decomposed into contributions from the adjacent elements and the i^{th} element as

$$\begin{aligned}\mathbf{SAT}_\mathrm{L}^i &= \mathsf{SAT}_\mathrm{L}^i\mathbf{u}_h^i + \mathsf{SAT}_\mathrm{LC}^i\mathbf{u}_h^{i-1},\\ \mathbf{SAT}_\mathrm{R}^i &= \mathsf{SAT}_\mathrm{R}^i\mathbf{u}_h^i + \mathsf{SAT}_\mathrm{RC}^i\mathbf{u}_h^{i+1},\end{aligned} \tag{25}$$

where $\mathsf{SAT}_\mathrm{L}^i$, $\mathsf{SAT}_\mathrm{LC}^i$, $\mathsf{SAT}_\mathrm{R}^i$, and $\mathsf{SAT}_\mathrm{RC}^i$ are $n \times n$ matrices. In this paper, we use the Baumann-Oden type interface SATs,[4,22] where the matrices in (25) are given by

$$\begin{aligned}\mathsf{SAT}_\mathrm{R}^i &= \sigma_1^\mathrm{R}\mathsf{H}^{-1}\mathsf{E}_{x_\mathrm{R}} + \sigma_2^\mathrm{R}\mathsf{H}^{-1}\mathsf{E}_{x_\mathrm{R}}\mathsf{B}^i\tilde{\mathsf{D}}_1 + \sigma_3^\mathrm{R}\mathsf{H}^{-1}\tilde{\mathsf{D}}_1^\mathrm{T}\mathsf{B}^i\mathsf{E}_{x_\mathrm{R}},\\ \mathsf{SAT}_\mathrm{RC}^i &= -\sigma_1^\mathrm{R}\mathsf{H}^{-1}\mathbf{t}_{x_\mathrm{R}}\mathbf{t}_{x_\mathrm{L}}^\mathrm{T} - \sigma_2^\mathrm{R}\mathsf{H}^{-1}\mathbf{t}_{x_\mathrm{R}}\mathbf{t}_{x_\mathrm{L}}^\mathrm{T}\mathsf{B}^{i+1}\tilde{\mathsf{D}}_1 - \sigma_3^\mathrm{R}\mathsf{H}^{-1}\tilde{\mathsf{D}}_1^\mathrm{T}\mathsf{B}^i\mathbf{t}_{x_\mathrm{R}}\mathbf{t}_{x_\mathrm{L}}^\mathrm{T},\\ \mathsf{SAT}_\mathrm{L}^i &= \sigma_1^\mathrm{L}\mathsf{H}^{-1}\mathsf{E}_{x_\mathrm{L}} + \sigma_2^\mathrm{L}\mathsf{H}^{-1}\mathsf{E}_{x_\mathrm{L}}\mathsf{B}^i\tilde{\mathsf{D}}_1 + \sigma_3^\mathrm{L}\mathsf{H}^{-1}\tilde{\mathsf{D}}_1^\mathrm{T}\mathsf{B}^i\mathsf{E}_{x_\mathrm{L}},\\ \mathsf{SAT}_\mathrm{LC}^i &= -\sigma_1^\mathrm{L}\mathsf{H}^{-1}\mathbf{t}_{x_\mathrm{L}}\mathbf{t}_{x_\mathrm{R}}^\mathrm{T} - \sigma_2^\mathrm{L}\mathsf{H}^{-1}\mathbf{t}_{x_\mathrm{L}}\mathbf{t}_{x_\mathrm{R}}^\mathrm{T}\mathsf{B}^{i-1}\tilde{\mathsf{D}}_1 - \sigma_3^\mathrm{L}\mathsf{H}^{-1}\tilde{\mathsf{D}}_1^\mathrm{T}\mathsf{B}^i\mathbf{t}_{x_\mathrm{L}}\mathbf{t}_{x_\mathrm{R}}^\mathrm{T}.\end{aligned} \tag{26}$$

The SAT parameters, σ_{x_L}, σ_{x_R}, and the σs in the interface coupling SATs above are chosen so that the resulting discretization is stable and conservative. For the numerical studies in this paper, the following

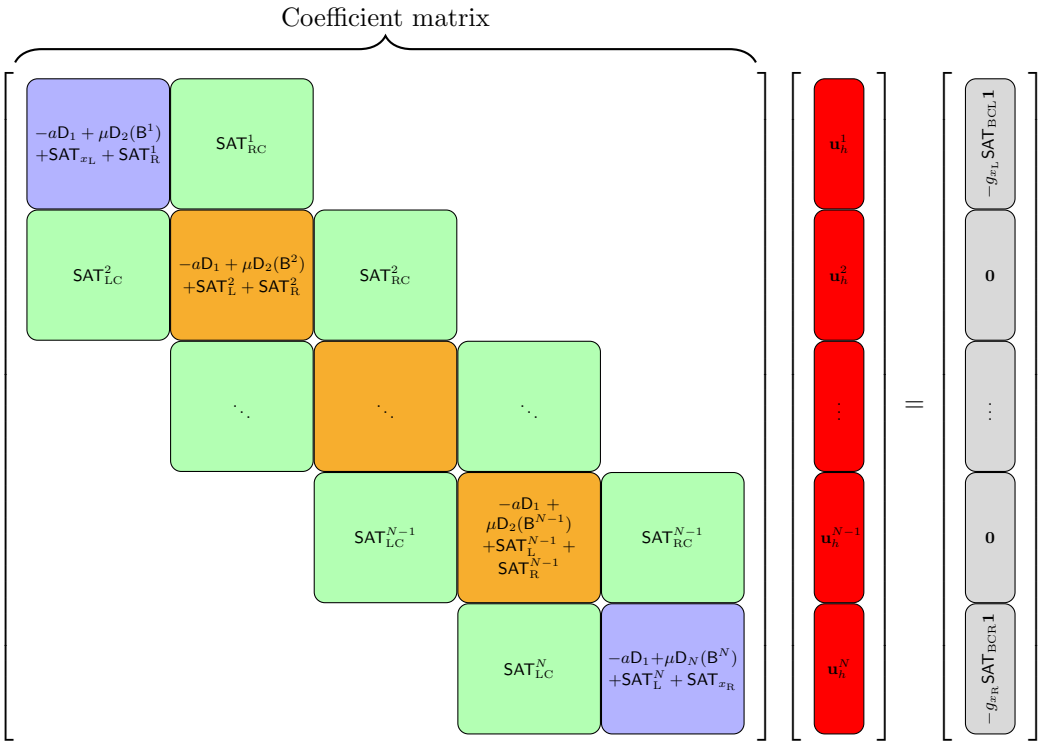

Figure 2: Schematic of the discretization of the linear convection-diffusion equation using the GSBP-SAT method.

values for the boundary condition and SAT parameters, based on the analysis in Ref. 22, are used:

$$\begin{gathered}
\alpha_{x_\mathrm{L}} = a \qquad \beta_{x_\mathrm{L}} = -\mu \qquad \alpha_{x_\mathrm{R}} = 0 \qquad \beta_{x_\mathrm{L}} = \mu \\
\sigma_{x_\mathrm{L}} = \frac{\mu}{\beta_{x_\mathrm{L}}} \qquad \sigma_{x_\mathrm{R}} = \frac{-\mu}{\beta_{x_\mathrm{R}}} \\
\sigma_1^\mathrm{R} = \tfrac{a}{2} \qquad \sigma_2^\mathrm{R} = \mu \qquad \sigma_3^\mathrm{R} = -\mu - \sigma_2^\mathrm{R} \\
\sigma_1^\mathrm{L} = \sigma_1^\mathrm{R} - a \quad \sigma_2^\mathrm{L} = \sigma_2^\mathrm{R} + \mu \qquad \sigma_3^\mathrm{L} = -\sigma_2^\mathrm{L}.
\end{gathered} \tag{27}$$

The full discretization is given in Figure 2.

V.A. SATs for GSBP operators

In Figure 2, the coupling SATs from adjacent elements, the green blocks in the coefficient matrix, appear as full matrices. However, the contribution from these SATs depends on whether the nodal distribution of the operator does or does not contain nodes that coincided with the boundaries of the element. As an example of the former, consider using the first-order classical SBP operator applied using the element approach, each element having five nodes. The nodal distribution for the i^{th} element is given by

$$\mathbf{x} = \frac{\Delta x}{4}\begin{bmatrix} 0 & 1 & 2 & 3 & 4 \end{bmatrix} + \Delta x(i-1) + x_\mathrm{L}, \tag{28}$$

and we can see that the first and last nodes coincide with the boundaries of the element, which for the i^{th} element are $x_\mathrm{L} + (i-1)\,\Delta x$ and $x_\mathrm{L} + i\,\Delta x$. The various matrices for the first-derivative operator are given

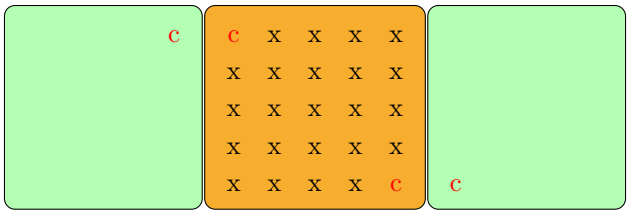

Figure 3: Coefficient matrix entries for an element on the interior of the domain discretized using first-order classical GSBP operators which have nodal distributions that contain nodes on the element boundaries. Entries with x originate from the discretization of the derivative terms, while c are entries modified by interface SATs

by

$$\mathsf{D}_1 = \frac{1}{h}\begin{bmatrix} -1 & 1 & & & \\ -\frac{1}{2} & 0 & \frac{1}{2} & & \\ & -\frac{1}{2} & 0 & \frac{1}{2} & \\ & & -\frac{1}{2} & 0 & \frac{1}{2} \\ & & & -1 & 1 \end{bmatrix}, \mathsf{H} = h\begin{bmatrix} \frac{1}{2} & & & & \\ & 1 & & & \\ & & 1 & & \\ & & & 1 & \\ & & & & \frac{1}{2} \end{bmatrix}, \mathsf{E} = \begin{bmatrix} -1 & & & & \\ & 0 & & & \\ & & 0 & & \\ & & & 0 & \\ & & & & 1 \end{bmatrix}, \mathbf{t}_{x_\mathrm{L}} = \begin{bmatrix} 1 \\ 0 \\ 0 \\ 0 \\ 0 \end{bmatrix}, \mathbf{t}_{x_\mathrm{R}} = \begin{bmatrix} 1 \\ 0 \\ 0 \\ 0 \\ 0 \end{bmatrix}, \tag{29}$$

where $h = \frac{\Delta x}{4}$. Furthermore,

$$\mathsf{E}_{x_\mathrm{L}} = \begin{bmatrix} 1 & & & & \\ & 0 & & & \\ & & 0 & & \\ & & & 0 & \\ & & & & 0 \end{bmatrix}, \mathsf{E}_{x_\mathrm{R}} = \begin{bmatrix} 0 & & & & \\ & 0 & & & \\ & & 0 & & \\ & & & 0 & \\ & & & & 1 \end{bmatrix}, \mathbf{t}_{x_\mathrm{L}}\mathbf{t}_{x_\mathrm{R}}^\mathrm{T} = \begin{bmatrix} & & & & 1 \\ & & & 0 & \\ & & 0 & & \\ & 0 & & & \\ 0 & & & & \end{bmatrix}, \mathbf{t}_{x_\mathrm{L}}\mathbf{t}_{x_\mathrm{R}}^\mathrm{T} = \begin{bmatrix} & & & & 0 \\ & & & 0 & \\ & & 0 & & \\ & 0 & & & \\ 1 & & & & \end{bmatrix}. \tag{30}$$

Figure 3 depicts the contribution to the coefficient matrix in Figure 2 from the i^{th} element. The entries c are those modified by the interface SATs, and we see that the coupling only occurs between the interface nodes.

Alternatively, consider a GSBP operator constructed on the five-node Chebyshev-Gauss quadrature nodes, which has a nodal distribution for the i^{th} element given by

$$\mathbf{x} = \frac{\Delta x}{2}\begin{bmatrix} -\cos\left(\frac{\pi}{10}\right) & -\cos\left(\frac{3\,\pi}{10}\right) & 0 & \cos\left(\frac{3\,\pi}{10}\right) & \cos\left(\frac{\pi}{10}\right) \end{bmatrix} + \frac{(2\,i-1)\Delta x}{2} + x_\mathrm{L}. \tag{31}$$

Notice that this nodal distribution does not contain nodes at the element boundaries. We now present the various matrix operators to five digits of accuracy required for the first-derivative operator and SATs; the second-derivative operator is presented in the next section. Those interested in obtaining this operator or any of the operators considered in this paper are encouraged to contact the primary author of this paper for the associated Matlab® scripts. The first derivative and norm matrix are given as

$$\mathsf{D}_1 = \frac{1}{h}\begin{bmatrix} -4.7470 & 6.5995 & -2.6537 & 1.0958 & -0.29504 \\ -1.1707 & -0.13012 & 1.7119 & -0.53792 & 0.11768 \\ 0.32485 & -1.3765 & 0.0 & 1.3765 & -0.32485 \\ -0.11768 & 0.53792 & -1.7119 & 0.13012 & 1.1707 \\ 0.29504 & -1.0958 & 2.6537 & -6.5995 & 4.7470 \end{bmatrix}, \mathsf{H} = h\begin{bmatrix} 0.30947 & 0.0 & 0.0 & 0.0 & 0.0 \\ 0.0 & 0.60063 & 0.0 & 0.0 & 0.0 \\ 0.0 & 0.0 & 0.37986 & 0.0 & 0.0 \\ 0.0 & 0.0 & 0.0 & 0.60063 & 0.0 \\ 0.0 & 0.0 & 0.0 & 0.0 & 0.30947 \end{bmatrix}, \tag{32}$$

where $h = \frac{\Delta x}{2}$. The matrices and vectors required for the SATs are given as

$$\mathsf{E} = \begin{bmatrix} -1.5933 & 0.49221 & -0.24621 & 0.11630 & 0.0 \\ 0.49221 & -0.14357 & 0.058086 & 0.0 & -0.11630 \\ -0.24621 & 0.058086 & 0.0 & -0.058086 & 0.24621 \\ 0.11630 & 0.0 & -0.058086 & 0.14357 & -0.49221 \\ 0.0 & -0.11630 & 0.24621 & -0.49221 & 1.5933 \end{bmatrix}, \mathbf{t}_{x_\mathrm{L}} = \begin{bmatrix} 1.2627 \\ -0.39237 \\ 0.20000 \\ -0.10194 \\ 0.031641 \end{bmatrix}, \mathbf{t}_{x_\mathrm{R}} = \begin{bmatrix} 0.031641 \\ -0.10194 \\ 0.20000 \\ -0.39237 \\ 1.2627 \end{bmatrix}, \tag{33}$$

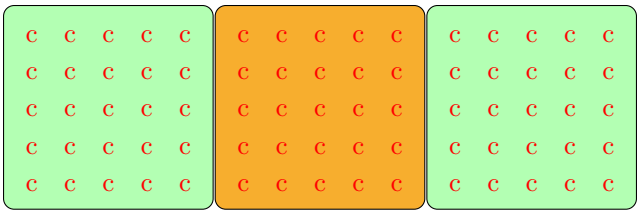

Figure 4: Coefficient matrix entries for an element on the interior of the domain discretized using the five-node Chebyshev-Gauss GSBP operators which have nodal distributions that do not contain nodes on the element boundaries. Entries with c are entries modified by interface SATs.

$$\mathsf{E}_{x_{\mathrm{L}}} = \begin{bmatrix} 1.59454 & -0.49566 & 0.25255 & -0.12868 & 0.04000 \\ -0.49566 & 0.15407 & -0.07850 & 0.04000 & -0.01243 \\ 0.25255 & -0.07850 & 0.04000 & -0.02038 & 0.00634 \\ -0.12868 & 0.04000 & -0.02038 & 0.01038 & -0.00323 \\ 0.04000 & -0.01243 & 0.00634 & -0.00323 & 0.00100 \end{bmatrix}, \mathsf{E}_{x_{\mathrm{R}}} = \begin{bmatrix} 0.00100 & -0.00323 & 0.00634 & -0.01243 & 0.04000 \\ -0.00323 & 0.01038 & -0.02038 & 0.04000 & -0.12868 \\ 0.00634 & -0.02038 & 0.04000 & -0.07850 & 0.25255 \\ -0.01243 & 0.04000 & -0.07850 & 0.15407 & -0.49566 \\ 0.04000 & -0.12868 & 0.25255 & -0.49566 & 1.59454 \end{bmatrix}, \quad (34)$$

$$\mathbf{t}_{x_{\mathrm{L}}}\mathbf{t}_{x_{\mathrm{R}}}^{\mathrm{T}} = \begin{bmatrix} 0.04000 & -0.12868 & 0.25255 & -0.49566 & 1.59454 \\ -0.01243 & 0.04000 & -0.07850 & 0.15407 & -0.49566 \\ 0.00634 & -0.02038 & 0.04000 & -0.07850 & 0.25255 \\ -0.00323 & 0.01038 & -0.02038 & 0.04000 & -0.12868 \\ 0.00100 & -0.00323 & 0.00634 & -0.01243 & 0.04000 \end{bmatrix}, \mathbf{t}_{x_{\mathrm{R}}}\mathbf{t}_{x_{\mathrm{L}}}^{\mathrm{T}} = \begin{bmatrix} 0.04000 & -0.01243 & 0.00634 & -0.00323 & 0.00100 \\ -0.12868 & 0.04000 & -0.02038 & 0.01038 & -0.00323 \\ 0.25255 & -0.07850 & 0.04000 & -0.02038 & 0.00634 \\ -0.49566 & 0.15407 & -0.07850 & 0.04000 & -0.01243 \\ 1.59454 & -0.49566 & 0.25255 & -0.12868 & 0.04000 \end{bmatrix}. \quad (35)$$

In contrast to classical SBP operators, which include boundary nodes, the matrices required for the SATs are not sparse. The contributions of the spatial discretization of the i^{th} element to the coefficient matrix is given in Figure 4 and we see that the interface SATs completely couple adjacent elements; therefore, all else equal, this makes such operators more expensive. However, as we will see in the results section, operators that do not include nodes at element boundaries can be constructed that are more efficient than operators that contain nodes at element boundaries . This results from the significant reduction in the truncation error that can be attained for such operators.

V.B. Implementation of compatible and order-matched operators

As discussed, compatible and order-matched operators can be constructed as

$$\mathsf{D}_2\left(\mathsf{B}\right) = \sum_{i=1}^{n} \mathsf{B}(i,i)\mathsf{M}_i. \quad (36)$$

Continuing the example using GSBP operators constructed on the five-node Chebyshev-Gauss quadrature nodes, the required matrices are given as

$$\mathsf{M}_1 = \frac{1}{h^2}\begin{bmatrix} 24.590 & -36.689 & 19.206 & -10.544 & 3.4383 \\ 5.4730 & -7.5024 & 2.8279 & -1.0568 & 0.25836 \\ -1.5876 & 2.2619 & -1.0070 & 0.47307 & -0.14037 \\ 0.69077 & -1.0568 & 0.59650 & -0.34703 & 0.11655 \\ -1.5550 & 2.3523 & -1.2846 & 0.72934 & -0.24200 \end{bmatrix}, \mathsf{M}_2 = \frac{1}{h^2}\begin{bmatrix} -7.5346 & -1.4131 & 11.966 & -4.0647 & 1.0462 \\ 0.25706 & -0.23531 & 0.079251 & -0.18040 & 0.079393 \\ 1.4854 & 0.51802 & -2.7708 & 1.0708 & -0.30344 \\ -0.50062 & -0.41297 & 1.3437 & -0.62918 & 0.19903 \\ 1.0462 & 0.77237 & -2.6522 & 1.2128 & -0.37914 \end{bmatrix}, \quad (37)$$

$$\mathsf{M}_3 = \frac{1}{h^2}\begin{bmatrix} -1.0178 & 4.0607 & -0.50192 & -3.2486 & 0.70764 \\ 0.68748 & -2.7025 & 0.41950 & 2.0237 & -0.42821 \\ -0.13730 & 0.35946 & -0.44432 & 0.35946 & -0.13730 \\ -0.42821 & 2.0237 & 0.41950 & -2.7025 & 0.68748 \\ 0.70764 & -3.2486 & -0.50192 & 4.0607 & -1.0178 \end{bmatrix}, \quad (38)$$

$$\mathsf{M}_4 = \frac{1}{h^2}\begin{bmatrix} -0.37914 & 1.2128 & -2.6522 & 0.77237 & 1.0462 \\ 0.19903 & -0.62918 & 1.3437 & -0.41297 & -0.50062 \\ -0.30344 & 1.0708 & -2.7708 & 0.51802 & 1.4854 \\ 0.079393 & -0.18040 & 0.079251 & -0.23531 & 0.25706 \\ 1.0462 & -4.0647 & 11.966 & -1.4131 & -7.5346 \end{bmatrix}, \mathsf{M}_5 = \frac{1}{h^2}\begin{bmatrix} -0.24200 & 0.72934 & -1.2846 & 2.3523 & -1.5550 \\ 0.11655 & -0.34703 & 0.59650 & -1.0568 & 0.69077 \\ -0.14037 & 0.47307 & -1.0070 & 2.2619 & -1.5876 \\ 0.25836 & -1.0568 & 2.8279 & -7.5024 & 5.4730 \\ 3.4383 & -10.544 & 19.206 & -36.689 & 24.590 \end{bmatrix}. \tag{39}$$

Finally, we also require the following matrix for the construction of the SATs (see (19) and (26)):

$$\tilde{\mathsf{D}}_1 = \frac{1}{h}\begin{bmatrix} -4.9798 & 7.2068 & -3.4026 & 1.7013 & -0.52573 \\ -1.0515 & -0.44903 & 2.1029 & -0.85065 & 0.24822 \\ 0.32492 & -1.3764 & 0.0 & 1.3764 & -0.32492 \\ -0.24822 & 0.85065 & -2.1029 & 0.44903 & 1.0515 \\ 0.52573 & -1.7013 & 3.4026 & -7.2068 & 4.9798 \end{bmatrix}. \tag{40}$$

If the PDE contains a time-varying variable coefficient, or is nonlinear and therefore requires a nonlinear solver, for example using pseudo time marching, then the sum in (36) needs to be reevaluated at each time step. Conversely, if the PDE contains a constant coefficient, i.e., we need only discretize a term of the form $\frac{\partial^2 \mathcal{U}}{\partial x^2}$, the sum $\sum_{i=1}^{n} \mathsf{M}_i$ is constructed once and for all, rather than evaluated at each time step.

For operators with a repeating interior point operator, we take advantage of the fact that such operators are sparse and instead of applying M_i we apply the nonzero sub-matrices. For the first-order classical SBP operator, on five nodes, the compatible and order-matched operator is given as

$$\mathsf{D}_2\left(\mathsf{B}\right) = \frac{1}{4\,h^2}$$
$$\begin{bmatrix} 10b_1 - 6b_2 & 8b_2 - 16b_1 & -2b_2 + 6b_1 & 0 & 0 \\ 4b_2 & 2b_1 - 2b_3 - 8b_2 & -2b_1 + 4b_2 + 2b_3 & 0 & 0 \\ -b_2 + b_1 & -2b_1 + 4b_2 + 2b_3 & -3b_2 - 3b_4 + b_1 - 4b_3 + b_5 & 2b_3 + 4b_4 - 2b_5 & -b_4 + b_5 \\ 0 & 0 & 2b_3 + 4b_4 - 2b_5 & -2b_3 + 2b_5 - 8b_4 & 4b_4 \\ 0 & 0 & -2b_4 + 6b_5 & 8b_4 - 16b_5 & -6b_4 + 10b_5 \end{bmatrix}. \tag{41}$$

In (41) the short form $b_i = \mathsf{B}(i,i)$ has been used. It is possible to construct the second derivative operator using the above form, which requires the evaluation of the individual entries in the matrix. This has the disadvantage that the variable coefficient needs to be accessed or constructed multiple times. The form (36) reduces the above to one loop, based on the variable coefficient, and is also advantageous for the construction of implicit methods that require the linearization of the compatible and order-matched GSBP operator, since the linearization is completely transparent. Now we reorganize (41) in terms of the variable coefficient using form (36), which leads to the following M_i matrices:

$$\mathsf{M}_1 = \frac{1}{4\,h^2}\begin{bmatrix} 10 & -16 & 6 & 0 & 0 \\ 0 & 2 & -2 & 0 & 0 \\ 1 & -2 & 1 & 0 & 0 \\ 0 & 0 & 0 & 0 & 0 \\ 0 & 0 & 0 & 0 & 0 \end{bmatrix}, 4h^2\mathsf{M}_2 = \begin{bmatrix} -6 & 8 & -2 & 0 & 0 \\ 4 & -8 & 4 & 0 & 0 \\ -1 & 4 & -3 & 0 & 0 \\ 0 & 0 & 0 & 0 & 0 \\ 0 & 0 & 0 & 0 & 0 \end{bmatrix}, \tag{42}$$

$$\mathsf{M}_3 = \frac{1}{4\,h^2}\begin{bmatrix} 0 & 0 & 0 & 0 & 0 \\ 0 & -2 & 2 & 0 & 0 \\ 0 & 2 & -4 & 2 & 0 \\ 0 & 0 & 2 & -2 & 0 \\ 0 & 0 & 0 & 0 & 0 \end{bmatrix}, \tag{43}$$

$$\mathsf{M}_4 = \frac{1}{4\,h^2}\begin{bmatrix} 0 & 0 & 0 & 0 & 0 \\ 0 & 0 & 0 & 0 & 0 \\ 0 & 0 & -3 & 4 & -1 \\ 0 & 0 & 4 & -8 & 4 \\ 0 & 0 & -2 & 8 & -6 \end{bmatrix}, \mathsf{M}_5 = \frac{1}{4\,h^2}\begin{bmatrix} 0 & 0 & 0 & 0 & 0 \\ 0 & 0 & 0 & 0 & 0 \\ 0 & 0 & 1 & -2 & 1 \\ 0 & 0 & -2 & 2 & 0 \\ 0 & 0 & 6 & -16 & 10 \end{bmatrix}. \tag{44}$$

Note that M_4 and M_5 are equal to the permutation of the rows and columns of M_2 and M_1, respectively. Instead of using the full M_i matrices, the operator can be constructed using only the nonzero sub-matrices. We define the following five matrices:

$$\begin{gathered} \mathsf{F}_1 := \mathsf{M}_1(1:3,1:3), \quad \mathsf{F}_2 := \mathsf{M}_2(1:3,1:3), \quad \mathsf{F}_3 := \mathsf{M}_3(2:4,2:4), \\ \mathsf{F}_4 := \mathsf{M}_4(3:5,3:5), \quad \mathsf{F}_5 := \mathsf{M}_5(3:5,3:5). \end{gathered} \tag{45}$$

The the second-derivative operator is constructed using the following four steps:

1. $\mathsf{D}_2 := \text{zeros}(n,n)$
2. $\mathsf{D}_2\,(\mathsf{B})\,(1:3,1:3) := b_1\mathsf{F}_1 + b_2\mathsf{F}_2$
3. $\mathsf{D}_2\,(\mathsf{B})\,(2:4,2:4) := \mathsf{D}_2\,(\mathsf{B})\,(2:4,2:4) + b_3\mathsf{F}_3$
4. $\mathsf{D}_2\,(\mathsf{B})\,(3:5,3:5) := \mathsf{D}_2\,(\mathsf{B})\,(3:5,3:5) + b_4\mathsf{F}_4 + b_5\mathsf{F}_5$,

To extend the above algorithm to more than five nodes, it is only necessary to change the indexing of the last matrix addition and add F_3 additional times. Thus, for n nodes, we have the following algorithm:

Algorithm 1 Pseudo code for constructing $\mathsf{D}_2\,(\mathsf{B})$ for a classical first-order compatible and order-matched SBP operator

$\mathsf{D}_2\,(\mathsf{B}) := \text{zeros}(n,n)$
$\mathsf{D}_2\,(\mathsf{B})\,(1:3,1:3) := b_1\mathsf{F}_1 + b_2\mathsf{F}_2$
for $i = 3 : n-2$ **do**
    $\mathsf{D}_2\,(\mathsf{B})\,(i-1:i+1,i-1:i+1) := \mathsf{D}_2\,(\mathsf{B})\,(i-1:i+1,i-1:i+1) + b_i\mathsf{F}_3$
end for
$\mathsf{D}_2\,(\mathsf{B})\,(n-2:n,n-2:n) := \mathsf{D}_2\,(\mathsf{B})\,(n-2:n,n-2:n) + b_{n-1}\mathsf{F}_4 + b_n\mathsf{F}_5$

The crucial observation is that we are simply adding F_3 additional times for additional nodes. In fact, F_3 is simply the contribution from the interior point operator.

VI. Summary of GSBP operators

We investigate two classes of operators: those with a repeating interior point operator and element-type operators constructed on the Chebyshev-Gauss and Legendre-Gauss-Lobatto quadrature nodes. For the former, we examine classical SBP operators and hybrid Gauss-trapezoidal-Lobatto (HGTL) and hybrid Gauss-trapezoidal (HGT) operators, which are derived on evenly spaced nodal distributions on the interior with a finite number of unequally spaced nodes near the boundaries; a similar family of operators has been derived by Mattsson et al.[23] Table 1 lists the abbreviations for the various GSBP operators used in this paper.[4] All of the operators used in this paper and many more are available in Matlab® script from the primary author via email. The arguments of the abbreviations can take the following values:

- F^2 for the application of the first-derivative operator twice or CO for compatible and order-matched operators
- *elem* denotes that the operator is applied using the element approach, while *trad* is an operator applied using the traditional finite-difference approach

Table 1: Abbreviations for GSBP operators

Abbreviation	Operator
$\mathrm{LGL}\big(\mathrm{F}^2, \mathrm{elem}, n, p\big)$	Diagonal-norm element-type GSBP operator constructed on the Legendre-Gauss-Lobatto quadrature nodes.
$\mathrm{CG}\big(\mathrm{F}^2 \text{ or } \mathrm{CO}, \mathrm{elem}, n, p\big)$	Diagonal-norm element-type GSBP operator constructed on the Chebyshev-Gauss quadrature nodes.
$\mathrm{CSBP}\big(\mathrm{F}^2 \text{ or } \mathrm{CO}, \mathrm{elem} \text{ or } \mathrm{trad}, n, p\big)$	Diagonal-norm classical SBP operator with a repeating interior point operator.
$\mathrm{HGTL}\big(\mathrm{F}^2 \text{ or } \mathrm{CO}, \mathrm{elem} \text{ or } \mathrm{trad}, n, p\big)$	Diagonal-norm GSBP operator on the hybrid Gauss-trapezoidal-Lobatto nodal distribution with a repeating interior point operator.
$\mathrm{HGT}\big(\mathrm{F}^2 \text{ or } \mathrm{CO}, \mathrm{elem} \text{ or } \mathrm{trad}, n, p\big)$	Diagonal-norm GSBP operator on the hybrid Gauss-trapezoidal nodal distribution with a repeating interior point operator.

- n is the number of nodes in each element (not applicable to operators applied using the traditional finite-difference approach)
- p is the order of the second-derivative operator

The order of operators for the first derivative, constructed on the Chebyshev-Gauss quadrature nodes with n nodes, is $\lceil \frac{n}{2} \rceil$ and for the application of the first-derivative operator twice is $\lceil \frac{n}{2} \rceil - 1$, where $\lceil \cdot \rceil$ is the ceiling operator which returns the closest integer greater than or equal to the argument. For compatible and order-matched operators, the order is $\lceil \frac{n}{2} \rceil$. The first-derivative operator constructed on the Legendre-Gauss-Lobatto quadrature nodes with n nodes has order $n-1$.[24] Using this nodal distribution, order-matched operators cannot be constructed, and we are therefore limited to the application of the first-derivative operator twice, which is of order $n-2$. For operators with a repeating interior point operator, applying a first-derivative operator of order p twice leads to an approximation to the second derivative of order $p-1$, while compatible and order-matched operators are of order p.

VII. Results

We solve the steady linear convection-diffusion equation (15) subject to boundary conditions (16). The variable coefficient in (15) is given by

$$\mathcal{B} = 2 + \sin(10x). \tag{46}$$

The physical constants are taken as $a = 1$ and $\mu = \frac{1}{10}$, while the problem is solved on the domain $x \in \left[\frac{32}{100}, \frac{94}{100}\right]$, and the source term $\mathcal{S}$ and the functions $\mathcal{G}_{x_\mathrm{L}}$ and $\mathcal{G}_{x_\mathrm{R}}$ are chosen such that the solution to (15) and (16) is

$$\mathcal{U}(x) = \exp\left(\frac{a}{\mu}\left(\frac{\tan^{-1}\left(\frac{2\tan(5x)+1}{\sqrt{3}}\right)}{5\sqrt{3}}\right)\right). \tag{47}$$

The solution error is defined by

$$\|\mathbf{e}\|_{\mathsf{H}} = \sqrt{\mathbf{e}^{\mathrm{T}}\bar{\mathsf{H}}\mathbf{e}}, \tag{48}$$

Table 2: Convergence of the solution error obtained using operators with a repeating interior point operator of order four implemented using the element approach or the traditional finite-difference approach

Operator	Order	Operator	Order
$\mathrm{CSBP}(\mathrm{F}^2, \mathrm{elem}, 13, 1)$	3.134	$\mathrm{CSBP}(\mathrm{F}^2, \mathrm{trad}, -, 1)$	2.9939
$\mathrm{CSBP}(\mathrm{CO}, \mathrm{elem}, 13, 2)$	3.534	$\mathrm{CSBP}(\mathrm{CO}, \mathrm{trad}, -, 2)$	4.2867
$\mathrm{HGT}(\mathrm{F}^2, \mathrm{elem}, 13, 1)$	3.0184	$\mathrm{HGT}(\mathrm{F}^2, \mathrm{trad}, -, 1)$	2.9815
$\mathrm{HGT}(\mathrm{CO}, \mathrm{elem}, 13, 2)$	3.8143	$\mathrm{HGT}(\mathrm{CO}, \mathrm{trad}, -, 2)$	4.2693

where $\mathbf{e} = (\mathbf{u}_h - \mathbf{u}_a)$, $\mathbf{u}_a$ is the restriction of the analytical solution onto the grid, and $\bar{\mathsf{H}}$ is a diagonal matrix with the norm matrix, H, from each element along the diagonal.

Tables 2 through 5 give the convergence rates of the solution error, which is computed by determining the slope of the line of best fit through the points $(x, y) = (\log(h), \log(\|\mathbf{e}\|_{\mathsf{H}}))$ associated with the filled-in markers in the figures. Figures 5 through 8 present the convergence of the $\|\mathbf{e}\|_{\mathsf{H}}$ versus $\frac{1}{\mathrm{DOF}}$ as well as the cpu time to compute the left-hand side (LHS) of the discretization, where DOF stands for degrees of freedom in the spatial operator. For operators implemented using the traditional finite-difference approach, DOF is the number of nodes and h is the average spacing between nodes, i.e., $\frac{x_{\mathrm{R}} - x_{\mathrm{L}}}{n-1}$. For element-type operators, DOF is the product of the number of elements and the number of nodes in each element and h is the size of the element. In this paper, grid refinement using the element approach is carried out by equally subdividing elements, starting with one element at the coarsest grid level, while grid refinement using the traditional finite-difference approach is carried out by doubling the number of nodes.

Tables 2 through 4 show that operators with a repeating interior point operator implemented using the traditional finite-difference approach have convergence rates of approximately the order of the operator plus two, which is in line with the theory of Svärd and Nordström.[25] In contrast, implementing these same operators using the element approach, the convergence rates of even-order compatible and order-matched operators are reduced. Examining Figures 5 through 7, we see that using the traditional finite-difference approach significantly reduces the global error and leads to more efficient schemes. We also see the significant advantage gained by considering operators that do not include boundary nodes, whether implemented using the element approach or the traditional finite-difference approach, despite the additional computational cost associated with the increased coupling from the SATs. Furthermore, compatible and order-matched operators have increased convergence rates, lower global error, and are more efficient than the application of the first-derivative operator twice. We find the hybrid Gauss-trapezoidal operators with interior point operators of order four and six and the Gauss-trapezoidal-Lobatto operator with an interior point operator of order eight to be more efficient than the classical SBP operators with equivalent order interior point operators constructed as either the application of the first-derivative operator twice or the compatible and order-matched versions.

Table 5 gives the convergence rates of the two families of element-type GSBP operators considered in this paper. For the Chebyshev-Gauss operators, the application of the first-derivative operator twice attains a convergence of the order of the operator plus two. In contrast, the Legendre-Gauss-Lobatto operators do not have this superconvergence and, in fact, do not even attain convergence rates of the order of the operator plus one. The compatible and order-matched Chebyshev-Gauss operator on five nodes has a convergence rate of the order of the operator plus one, while the seven-node operator does not attain this level of convergence. In Figure 8, we see that both five-node Chebyshev-Gauss operators are more efficient than the Legendre-Gauss-Lobatto operator, with the compatible and order-matched operator being the most efficient of the three. In that same figure, we find that both seven-node Chebyshev-Gauss operators are as efficient as the Legendre-Gauss-Lobatto operator. Finally, all of the compatible and order-matched operators with a repeating interior point operator, implemented as elements, are more efficient than the Legendre-Gauss-Lobatto operators.

We note that one possible reason for the under-convergence rates by either operators with a repeating interior point operator implemented using the element approach or the element-type operators may be a result of using the Baumann-Oden[26] interface SATs, which have previously been shown to lead to suboptimal convergence rates for pseudo-spectral operators.[27,28]

Table 3: Convergence of the solution error obtained using operators with a repeating interior point operator of order six implemented using the element approach or the traditional finite-difference approach

Operator	Order	Operator	Order
$\mathrm{CSBP}(\mathrm{F}^2, \mathrm{elem}, 19, 2)$	4.027	$\mathrm{CSBP}(\mathrm{F}^2, \mathrm{trad}, -, 2)$	3.9855
$\mathrm{CSBP}(\mathrm{CO}, \mathrm{elem}, 19, 3)$	4.8954	$\mathrm{CSBP}(\mathrm{CO}, \mathrm{trad}, -, 3)$	5.0286
$\mathrm{HGT}(\mathrm{F}^2, \mathrm{elem}, 19, 2)$	3.8703	$\mathrm{HGT}(\mathrm{F}^2, \mathrm{trad}, -, 2)$	3.7329
$\mathrm{HGT}(\mathrm{CO}, \mathrm{elem}, 19, 3)$	5.2723	$\mathrm{HGT}(\mathrm{CO}, \mathrm{trad}, -, 3)$	4.9415

Table 4: Convergence of the solution error obtained using operators with a repeating interior point operator of order eight implemented using the element approach or the traditional finite-difference approach

Operator	Order	Operator	Order
$\mathrm{CSBP}(\mathrm{F}^2, \mathrm{elem}, 25, 3)$	5.3374	$\mathrm{CSBP}(\mathrm{F}^2, \mathrm{trad}, -, 3)$	5.8418
$\mathrm{CSBP}(\mathrm{CO}, \mathrm{elem}, 25, 4)$	5.7061	$\mathrm{CSBP}(\mathrm{CO}, \mathrm{trad}, -, 4)$	6.1933
$\mathrm{HGT}(\mathrm{F}^2, \mathrm{elem}, 25, 3)$	5.4085	$\mathrm{HGT}(\mathrm{F}^2, \mathrm{trad}, -, 3)$	5.0517
$\mathrm{HGT}(\mathrm{CO}, \mathrm{elem}, 25, 4)$	5.5649	$\mathrm{HGT}(\mathrm{CO}, \mathrm{trad}, -, 4)$	5.8663

Table 5: Convergence of the solution error obtained using element-type operators

Operator	Order	Operator	Order
$\mathrm{CG}(\mathrm{F}^2, \mathrm{elem}, 5, 2)$	3.9836	$\mathrm{CG}(\mathrm{CO}, \mathrm{elem}, 5, 3)$	3.8073
$\mathrm{CG}(\mathrm{F}^2, \mathrm{elem}, 7, 3)$	3.9836	$\mathrm{CG}(\mathrm{CO}, \mathrm{elem}, 7, 4)$	3.8073
$\mathrm{LGL}(\mathrm{F}^2, \mathrm{elem}, 4, 3)$	3.1959	$\mathrm{LGL}(\mathrm{F}^2, \mathrm{elem}, 5, 4)$	3.1959

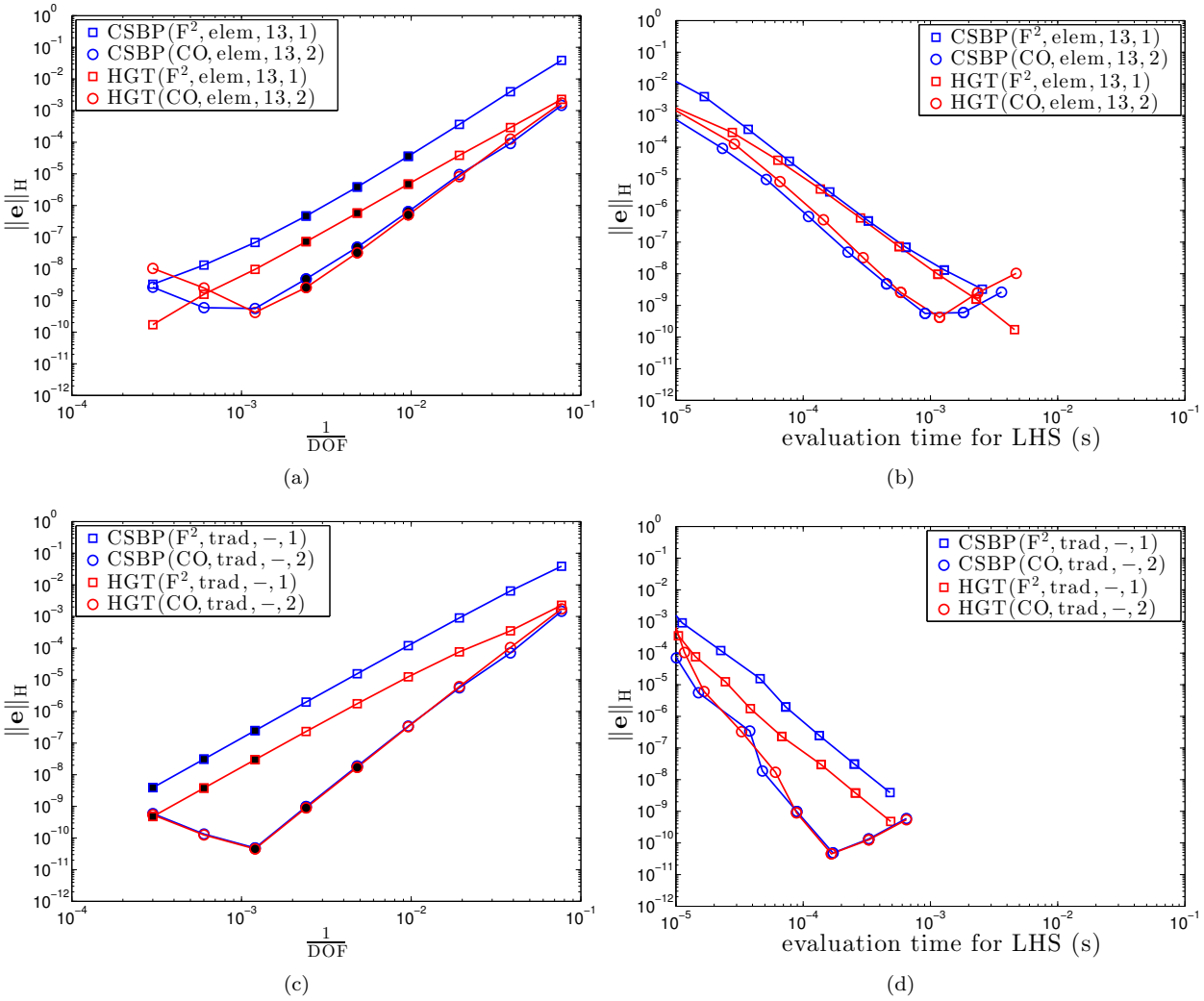

Figure 5: Solution error obtained using operators with a repeating interior point operator of order four implemented using the element approach or the traditional finite-difference approach. H norm of the error in the solution to problem (15) versus $\frac{1}{\text{DOF}}$, (a) and (c), or versus cpu time to construct the LHS, (b) and (d).

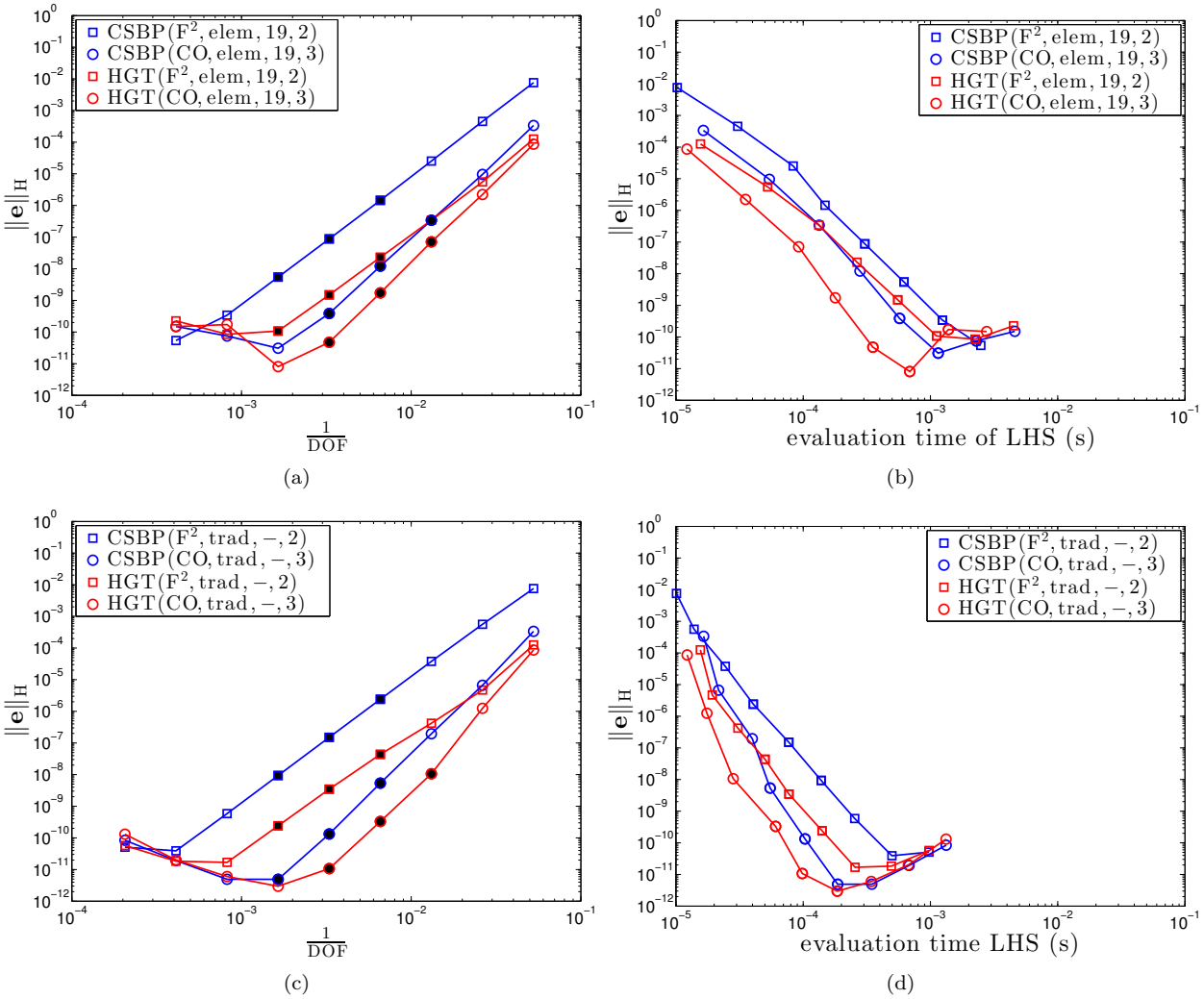

Figure 6: Solution error obtained using operators with a repeating interior point operator of order six using the element approach or the traditional finite-difference approach. H norm of the error in the solution to problem (15) versus $\frac{1}{\text{DOF}}$, (a) and (c), or versus cpu time to construct the LHS, (b) and (d).

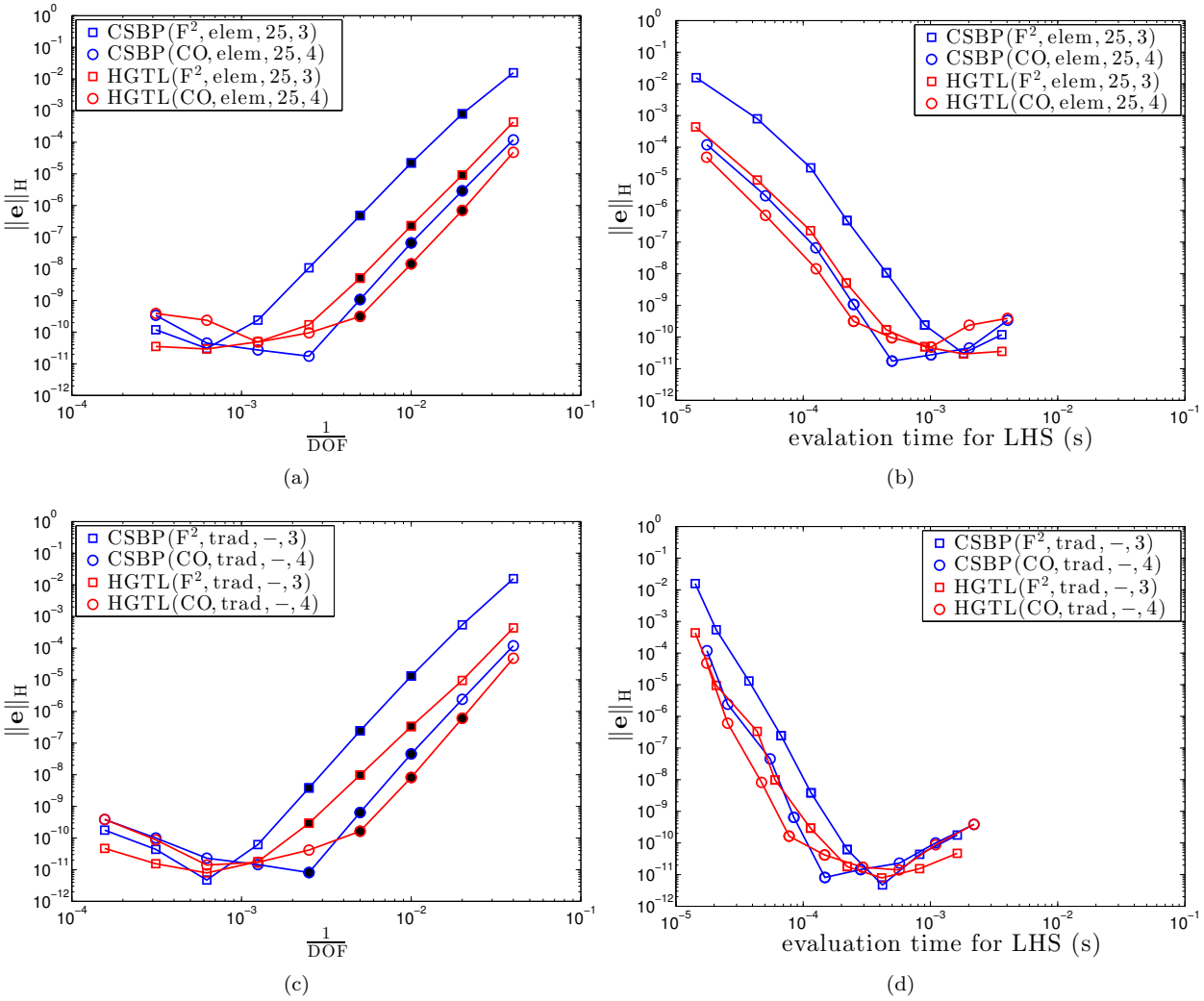

Figure 7: Solution error obtained using operators with a repeating interior point operator of order eight implemented using the element approach or the traditional finite-difference approach. H norm of the error in the solution to problem (15) versus $\frac{1}{\text{DOF}}$, (a) and (c), or versus cpu time to construct the LHS, (b) and (d).

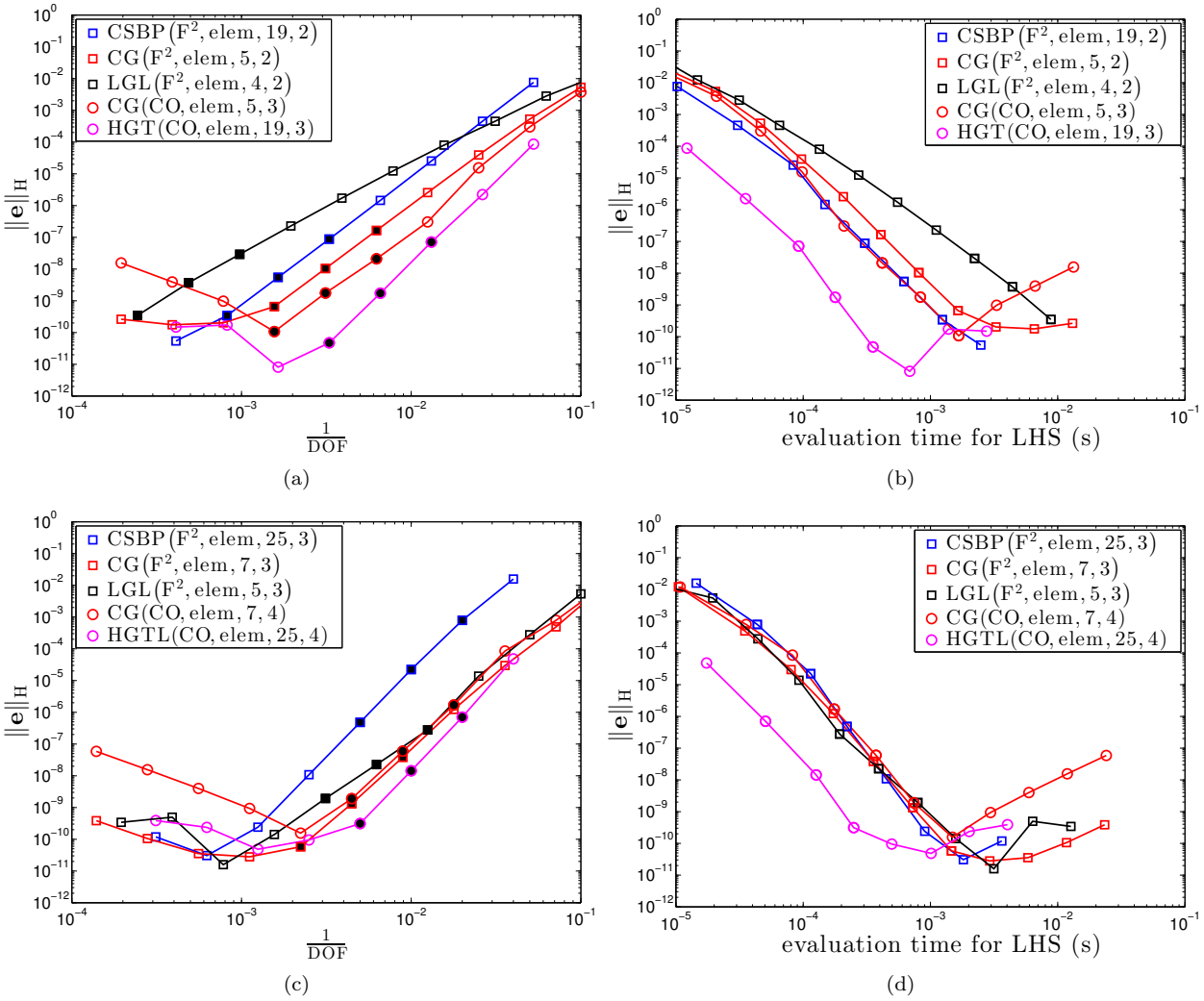

Figure 8: Comparison of various second-derivative operators of order two and three, (a) and (b), or three and four, (c) and (d). H norm of the error in the solution to problem (15) versus $\frac{1}{DOF}$, (a) and (c) or versus cpu time to construct the LHS, (b) and (d). The first-derivative operator in (a) and (b) is of order three and therefore the application of the first-derivative operator is of order two, while for (c) and (d) the first-derivative operator is of order four and therefore the application of the first-derivative twice is of order three.

VIII. Conclusions and future work

The results in Section VII show that compatible and order-matched GSBP and classical SBP operators can be more efficient than the application of the first-derivative operator twice. Several operators have been presented in detail to enable other researchers to implement them. We are particularly interested in examining the potential efficiency benefits of compatible and order-matched SBP second-derivative operators in the numerical solution of the Navier-Stokes equations. Recently Hicken et. al[29] have extended the GSBP framework to multi-dimensional operators with the SBP property on simplices. Such operators can be applied in the context of unstructured grids and in future work, we look to extend the idea of compatible and order-matched second-derivative operators with the SBP property to simplices.

References

[1]Del Rey Fernández, D. C., Boom, P. D., and Zingg, D. W., "A generalized framework for nodal first derivative summation-by-parts operators," *Journal of Computational Physics*, Vol. 266, No. 1, 2014, pp. 214–239.

[2]Boom, P. D. and Zingg, D. W., "High-Order Implicit Time-Marching Methods Based on Generalized Summation-By-Parts Operators," *Submitted to SIAM Journal on Scientific Computing, (see arXiv:1410.0201[Math.NA])*, 2014.

[3]Boom, P. D. and Zingg, D. W., "Runge-Kutta Characterization of the Generalized Summation-by-Parts Approach in Time," *Submitted to SIAM Journal on Scientific Computing, (see arXiv:1410.0202[Math.NA])*, 2014.

[4]Del Rey Fernández, D. C. and Zingg, D. W., "Generalized summation-by-parts operators for the second derivative with a variable coefficient," *Submitted to SIAM Journal on Scientific Computing, (see arXiv:1410.0201[Math.NA])*, 2014.

[5]Kreiss, H.-O. and Scherer, G., "Finite element and finite difference methods for hyperbolic partial differential equations," *Mathematical aspects of finite elements in partial differential equations*, Academic Press, New York/London, 1974, pp. 195–212.

[6]Strand, B., "Summation by parts for finite difference approximations for d/dx," *Journal of Computational Physics*, Vol. 110, No. 1, 1994, pp. 47–67.

[7]Carpenter, M. H., Gottlieb, D., and Abarbanel, S., "Time-stable boundary conditions for finite-difference schemes solving hyperbolic systems: Methodology and application to high-order compact schemes," *Journal of Computational Physics*, Vol. 111, No. 2, 1994, pp. 220–236.

[8]Carpenter, M. H., Nordström, J., and Gottlieb, D., "A stable and conservative interface treatment of arbitrary spatial accuracy," *Journal of Computational Physics*, Vol. 148, No. 2, 1999, pp. 341–365.

[9]Nordström, J. and Carpenter, M. H., "Boundary and interface conditions for high-order finite-difference methods applied to the Euler and Navier-Stokes equations," *Journal of Computational Physics*, Vol. 148, No. 2, 1999, pp. 621–645.

[10]Nordström, J. and Carpenter, M. H., "High-order finite-difference methods, multidimensional linear problems, and curvilinear coordinates," *Journal of Computational Physics*, Vol. 173, No. 1, 2001, pp. 149–174.

[11]Mattsson, K. and Nordström, J., "Summation by parts operators for finite difference approximations of second derivatives," *Journal of Computational Physics*, Vol. 199, 2004, pp. 503–540.

[12]Mattsson, K., "Summation by parts operators for finite difference approximations of second-derivatives with variable coefficients," *Journal of Scientific Computing*, Vol. 51, No. 3, 2012, pp. 650–682.

[13]Svärd, M. and Nordström, J., "Review of summation-by-parts schemes for initial-boundary-value-problems," *Journal of Computational Physics*, Vol. 268, No. 1, 2014, pp. 17–38.

[14]Del Rey Fernández, D. C., Hicken, J. E., and Zingg, D. W., "Review of summation-by-parts operators with simultaneous approximation terms for the numerical solution of partial differential equations," *Computers & Fluids*, Vol. 95, No. 22, 2014, pp. 171–196.

[15]Gustafsson, B., *High Order Difference Methods for Time Dependent PDE*, Springer, 2008.

[16]Gustafsson, B., Kreiss, H.-O., and Oliger, J., *Time-Dependent Problems and Difference Methods*, Pure and Applied Mathematics, Wiley, 2nd ed., 2013.

[17]Kreiss, H.-O. and Lorenz, J., *Initial-Boundary Value Problems and the Navier-Stokes Equations*, Vol. 47 of *Classics in Applied Mathematics*, SIAM, 2004.

[18]Del Rey Fernández, D. C. and Zingg, D. W., "New diagonal-norm summation-by-parts operators for the first derivative with increased order of accuracy," *AIAA aviation 2015*, 2014.

[19]Mattsson, K. and Almquist, M., "A solution to the stability issues with block norm summation by parts operators," *Journal of Computational Physics*, Vol. 15, 2013, pp. 418–442.

[20]Mattsson, K., Svärd, M., and Shoeybi, M., "Stable and accurate schemes for the compressible Navier-Stokes equations," *Journal of Computational Physics*, Vol. 227, No. 4, 2008, pp. 2293–2316.

[21]Kamakoti, R. and Pantano, C., "High-order narrow stencil finite-difference approximations of second-derivatives involving variable coefficients," *SIAM Journal on Scientific Computing*, Vol. 31, No. 6, 2009, pp. 4222–4243.

[22]Gong, J. and Nordström, J., "Interface Procedures for Finite Difference Approximations of the advection-diffusion equation," *Journal of Computational and Applied Mathematics*, Vol. 236, 2011, pp. 602–620.

[23]Mattsson, K., Almquist, M., and Carpenter, M. H., "Optimal diagonal-norm SBP operators," *Journal of Computational Physics*, Vol. 264, No. 1, 2014, pp. 91–111.

[24]Shen, J., Tang, T., and Wang, L.-L., *Spectral methods algorithms, analysis and applications*, Springer, 2011.

[25]Svärd, M. and Nordström, J., "On the order of accuracy for difference approximation of initial-boundary value problems," *Journal of Computational Physics*, Vol. 218, No. 1, 2006, pp. 333–352.

[26]Baumann, C. E. and Oden, J. T., "A discontinuous hp finite element method for convection-diffusion problems," *Computer Methods in Applied Mechanics and Engineering*, Vol. 175, No. 3-4, 1999, pp. 311–341.

[27]Carpenter, M. H., Nordström, J., and Gottlieb, D., "Revisiting and Extending Interface Penalties for Multi-domain Summation-by-Parts Operators," Tech. rep., NASA Langley Research Center, 2007.

[28]Carpenter, M. H., Nordström, J., and Gottlieb, D., "Revisiting and Extending Interface Penalties for Multi-domain Summation-by-Parts Operators," *Journal of Scientific Computing*, Vol. 45, No. 1-3, 2010, pp. 118–150.

[29]Hicken, J. E., Del Rey Fernández, D. C., and Zingg, D. W., "Multidimensional summation-by-part operators: General theory and application to simplex elements," *Submitted to the Journal of Computational Physics (2015). (see arXiv:1505.03125v1[math.NA])*, 2015.